energies

MDPI

Article

Feedback Linearization Controller for a Wind Energy Power System

Muthana Alrifai *, Mohamed Zribi and Mohamed Rayan

Department of Electrical Engineering, Kuwait University, P. O. Box 5969, Safat 13060, Kuwait; mohamed.zribi@ku.edu.kw (M.Z.); mmsrayan@gmail.com (M.R.)
* Correspondence: m.alrifai@ku.edu.kw; Tel.: +965-2498-7381

Academic Editor: Paolo Mercorelli
Received: 14 June 2016; Accepted: 19 September 2016; Published: 23 September 2016

Abstract: This paper deals with the control of a doubly-fed induction generator (DFIG)-based variable speed wind turbine power system. A system of eight ordinary differential equations is used to model the wind energy conversion system. The generator has a wound rotor type with back-to-back three-phase power converter bridges between its rotor and the grid; it is modeled using the direct-quadrature rotating reference frame with aligned stator flux. An input-state feedback linearization controller is proposed for the wind energy power system. The controller guarantees that the states of the system track the desired states. Simulation results are presented to validate the proposed control scheme. Moreover, further simulation results are shown to investigate the robustness of the proposed control scheme to changes in some of the parameters of the system.

Keywords: wind energy; doubly-fed induction generator (DFIG); feedback linearization

1. Introduction

There has been a global interest in renewable energy resources due to the worldwide increase in power demand and the limitation of fossil fuels and their harmful impact on the environment. Renewable energy resources, such as wind energy, are naturally available, clean and have a much less harmful impact on the environment than fossil fuels.

Wind energy is the fastest growing renewable energy resource. Globally, the annual cumulative installed wind energy capacity has increased rapidly during the period from 1997–2014 [1]. In addition, the advancement on the design of the components of wind energy power systems that include power electronics inverters, electric generators and drive train systems has also contributed to the fast growth and high demand of wind energy conversion systems (WECs). The increasing market share of variable speed wind energy conversion systems has led to further investigations of wind turbines' control technology. Furthermore, researchers have recognized that appropriate control algorithms can greatly improve the efficiency of wind power conversion systems.

Among the various types of available wind turbines, the doubly-fed induction generator-based wind turbines are widely used for variable speed wind turbine systems because of their simple structures, their reliable operations, their high power densities and their energy efficiency. Moreover, doubly-fed induction generators-based energy systems have other advantages, such as the reduction of mechanical stress, the flexibility in controlling active and reactive powers and the ability to track maximum power using different control techniques.

Many research articles dealing with the design of different types of control schemes for DFIG-based variable speed wind turbine systems were published in the last few years; for example, the reader can refer to the works in [2–16] for a detailed review of wind turbine systems and their control. Some of these control techniques are highlighted below.

Researchers have used different control techniques to control DFIG-based wind turbine energy systems. For example, PID controllers and several modified PID control schemes were used to control wind energy conversion systems [17–19]. These types of schemes are believed to be the easiest and simplest design methods. However, DFIG-based wind energy systems are highly nonlinear systems, which are characterized by strong couplings between the different variables of the systems. Thus, nonlinear control schemes need to be designed to control wind energy power systems so that the desired performances are attained.

The work in [20] proposed a method for obtaining the maximum power output of a DFIG-based wind energy system. The proposed control technique was based on the usage of an improved maximum power point tracking (MPPT) curve method and a Lyapunov function. In [21], an artificial neural network technique based on Markov scheme approaches was developed to optimize the output of a wind turbine system. An artificial neural network, which is based on the Jordan re-current concept, was used to estimate the reference tracking speed of the rotor in [22]. A direct and an indirect control structure using a quantum neural network to enhance the efficiency of the system and to optimize the output of a wind energy power system was proposed in [23]. Furthermore, the combination of fuzzy logic control and sliding mode control was investigated in the literature; for example, refer to the works in [24–28].

Investigations to determine the best nonlinear control technique that can be used to improve the performance of DFIG-based WEC systems are still ongoing [29]. The control of both the grid side converter (GSC) and the rotor side converter (RCS) in one control loop was reported in [30]. In [31], a direct active power and reactive power controller based on the estimation of the stator flux was proposed, and a basic hysteresis controller was used. Vector control and direct power control were proposed in [32] to regulate the active power and reactive power generated by a DFIG-based wind energy system. In [33], two distinct control strategies were used to control a DFIG-based WEC system; backstepping and sliding mode control strategies were first used to control the rotor side converter (RCS); then, the same strategies were used to control the grid side converter (GSC). A perturbation observer-based control scheme for the control of DFIG in a multi-machine power system was introduced in [34]. The controller is achieved with a four-loop perturbation observer-based control configuration, and the controlled dynamics were investigated through simulation studies.

Several researchers investigated the usage of the feedback linearization technique for the control of DFIG-based WEC systems. Some of these works are highlighted below. An input-output feedback linearization controller for a DFIG-based system connected to an infinite bus was discussed in [35]; the authors differentiated the electromagnetic torque, the stator power and the grid side converter power outputs of the DFIG to obtain a linear relationship with the rotor voltages, which serve as control inputs. Then, decoupled torque control and decoupled power control were developed. In [36], an input-output linearizing and decoupling control strategy was proposed for a doubly-fed induction generator system. The developed controller was verified by using a 7.5 kW wind power test rig. A mathematical model of the DFIG based on the so-called stator magnetizing current field orientation was given in [37]; then, an input-output linearizing controller is proposed. The controller results in decoupled control and the tracking of the generated active and reactive powers of the system. Direct control of the torque and direct control of the power outputs of the DFIG were established based on the input-output feedback linearization technique in [38,39]. In [40], an adaptive nonlinear control strategy based on a feedback linearization scheme was proposed for a DFIG-based WEC system; a disturbance observer was added to estimate the uncertainties in the parameters of the system. The performance of the system is checked in the presence of nearby faults. Moreover, an exact feedback linearization scheme was proposed in [41] for a DFIG-based WEC system. The wind turbine with DFIG is represented by a third-order model. This model is exactly linearized, and a linear quadratic regulator is used to design an optimal controller for the linearized system. Simulations were performed on a single machine infinite bus system and on a four-machine system; the simulation results indicate that the proposed control scheme improves the transient stability of the power system, and it enhances the damping of the system.

The contribution of this paper involves the design of an input-state feedback linearization controller for a wind energy conversion system. Previous works on feedback linearization of WEC systems, generally, used fifth order models or sixth order models. Our work uses an eighth order model of the WEC system; the state space representation of the eighth order model under consideration uses four electrical states and four mechanical states. The proposed controller controls the rotor side converter (RCS) of a DFIG. It guarantees the stability of the closed loop system and enables the tracking of the desired states of the system. In addition, the proposed controller maximizes the power extracted from the wind. The proposed theoretical work is verified through MATLAB simulations; moreover, the validity of the proposed controller was tested when some of the parameters of the system change.

The rest of the paper is organized as follows. Section 2 presents the model of a DFIG-based wind energy power system; the system consists of eight nonlinear ordinary differential equations. In Section 3, the computations of the values of the desired states of the system, as well as the reference inputs are discussed in detail. Section 4 presents the design of an input-state feedback linearization controller for the wind energy conversion system. To show the effectiveness of the proposed controller, simulation studies are presented in Section 5. In addition, some simulation results are shown to investigate the robustness of the controller to changes in some of the parameters of the system. Finally, the conclusion is drawn in Section 6.

2. Model of the Wind Energy Conversion System

The model of a DFIG-based wind energy conversion power system is presented in this section. A block diagram depiction of the system is shown in Figure 1. The system consists of a wind turbine connected through a gear box to a doubly-fed induction generator. The stator windings of the standard wound induction generator are directly connected to the grid. The rotor windings are connected to the grid through a voltage source and power electronics converters (AC/DC/AC). The wind energy is captured by the motor blades and transferred to the motor hub. The hub has a gearbox, which attaches the low-speed shaft to the high-speed shaft that drives the DFIG, which converts the mechanical energy to electrical energy. This electrical energy is delivered to the grid.

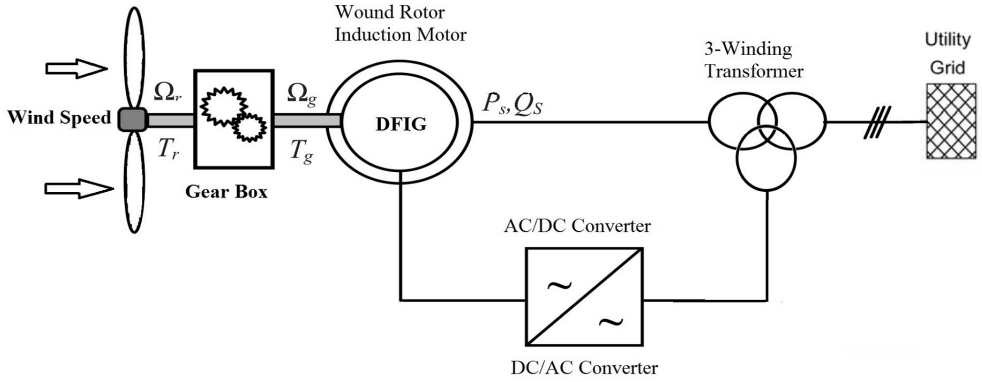

Figure 1. A block diagram representation of the variable speed DFIG-based wind energy conversion system.

Note that Ω_r, Ω_g, T_h and T_g depicted in Figure 1 represent the rotational speed of the turbine on the low-speed side of the gearbox, the mechanical speed of the generator, the high-speed shaft torque and the generator torque, respectively. Furthermore P_s and Q_s are the stator active power and the stator reactive power.

The mechanical power extracted from the wind can be expressed as [42],

$$P_m = \frac{1}{2} C_p(\lambda, \beta) \rho \pi R^2 V^3 \quad (1)$$

where:

P_m: the captured wind power (the mechanical power),
$C_p(\lambda, \beta)$: the power coefficient,
λ: the tip speed ratio (TSR),
β: the pitch angle,
ρ: the air density,
R: the rotor-plane radius,
V: the speed of the wind.

The tip speed ratio can be expressed as,

$$\lambda = \Omega_r R / V \tag{2}$$

where Ω_r is the rotational speed of the turbine on the low-speed side of the gearbox.

The power coefficient C_p versus the tip speed ratio λ for different values of the pitch angle β is depicted in Figure 2. It can be seen from the figure that when $\beta = 0$, the maximum value of C_p is achieved when $C_{p(\max)} = 0.48$ at an optimal value of the tip speed ratio $\lambda_{opt} = 8$. To capture the maximum power from the wind, a variable speed wind turbine normally follows the $C_{p(\max)}$ up to the rated speed by varying the rotor speed to keep the tip speed ratio at its optimum value λ_{opt}.

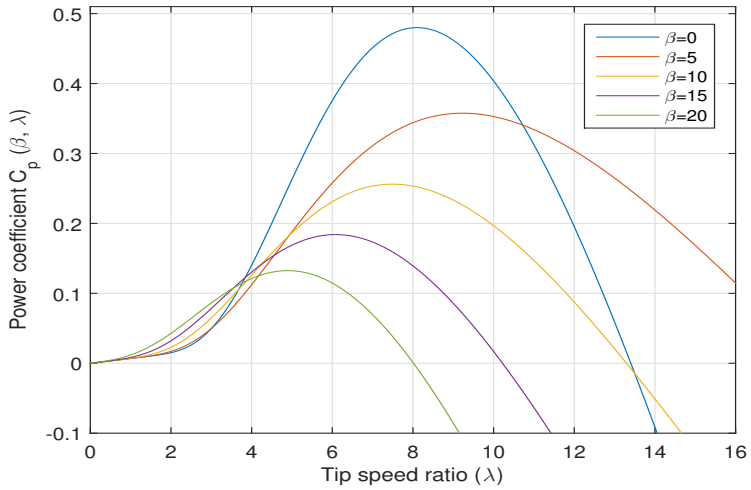

Figure 2. The power coefficient C_p versus the tip speed ratio λ.

Using Equation (1), the maximum captured wind power, $P_{m(\max)}$, can be written as,

$$P_{m(\max)} = \frac{1}{2} C_{p(\max)}(\lambda_{opt}, \beta) \rho \pi R^2 V^3. \tag{3}$$

The aerodynamic torque, T_r, can be expressed as follows,

$$T_r = P_m / \Omega_r = \frac{1}{2} C_p(\lambda, \beta) \rho \pi R^2 V^3 / \Omega_r. \tag{4}$$

The wind turbine varies its speed by following the maximum value of the power coefficient $C_{p(\max)}$ so that maximum power is captured. This is done by changing the speed of the rotor to maintain the tip speed ratio at its optimum value λ_{opt} [42]. Using Equations (2)–(4), the aerodynamic torque, T_r, can be written as follows,

$$T_r = K_{opt} \Omega_r^2 \tag{5}$$

where $K_{opt} = 0.5\rho\pi R^5 C_{p(\max)}/\lambda_{opt}^3$.

To model the wind energy power system, we first need to define the state variables of the system. The system consists of an electrical part and a mechanical part. The state variables of the electrical part of the system are the stator currents in the d and q axes (i_{sd} and i_{sq}) and the rotor currents in the d and q axes (i_{rd} and i_{rq}). The state variables of the mechanical part of the system are the rotational speed of the turbine on the low-speed side of the gearbox (Ω_r), the mechanical speed of the generator (Ω_g), the high-speed shaft torque (T_h) and the generator torque (T_g). The inputs for the system are the stator and rotor voltages and the required generator torque ($T_{g,r}$). Note that the voltage u_{sd} is the d-axis stator voltage, and u_{sq} is the q-axis stator voltage. The voltage u_{rd} is the d-axis rotor voltage, and u_{rq} is the q-axis rotor voltage.

The rotational speed of the generator Ω_g is related to the rotor angular frequency ω_r, such that,

$$\Omega_g = \frac{1}{n_p}\omega_r \tag{6}$$

where n_p is the number of pole pairs of the generator.

The stator angular frequency ω_s is related to the stator frequency, f_s, such that,

$$\omega_s = 2\pi f_s. \tag{7}$$

Furthermore, the leakage coefficient can be written, such that,

$$\xi = \frac{1 - L_m^2}{L_s L_r} \tag{8}$$

where L_m is the magnetizing inductance, L_r is the rotor leakage inductance and L_s is the stator leakage inductance.

The model of the wind energy power system consists of eight first order ordinary differential equations (odes). The first four odes are related to the electrical part of the system; the second four odes are related to the mechanical part of the system. Hence, the wind turbine energy conversion system can be described using the following set of nonlinear ordinary differential equations, such that [42,43],

$$\begin{aligned}
\frac{di_{sd}}{dt} &= \frac{-R_s}{\xi L_s} i_{sd} + \omega_s i_{sq} + \frac{1-\xi}{\xi} n_p \Omega_g i_{sq} + \frac{R_r L_m}{\xi L_r L_s} i_{rd} + \frac{L_m}{\xi L_s} n_p i_{rq} \Omega_g - \frac{1}{\xi L_s} u_{sd} + \frac{L_m}{\xi L_r L_s} u_{rd} \\
\frac{di_{sq}}{dt} &= -\omega_s i_{sd} - \frac{1-\xi}{\xi} n_p \Omega_g i_{sd} + \frac{-R_s}{\xi L_s} i_{sq} - \frac{L_m}{\xi L_s} n_p \Omega_g i_{rd} + \frac{R_r L_m}{\xi L_r L_s} i_{rq} - \frac{1}{\xi L_s} u_{sq} + \frac{L_m}{\xi L_r L_s} u_{rq} \\
\frac{di_{rd}}{dt} &= \frac{R_s L_m}{\xi L_r L_s} i_{sd} - \frac{L_m}{\xi L_r} n_p \Omega_g i_{sq} - \frac{R_r}{\xi L_r} i_{rd} + \omega_s i_{rq} - \frac{1}{\xi} n_p \Omega_g i_{rq} + \frac{L_m}{\xi L_r L_s} u_{sd} - \frac{1}{\xi L_r} u_{rd} \\
\frac{di_{rq}}{dt} &= \frac{L_m}{\xi L_r} n_p \Omega_g i_{sd} + \frac{R_s L_m}{\xi L_r L_s} i_{sq} - \omega_s i_{rd} + \frac{1}{\xi} n_p \Omega_g i_{rd} - \frac{R_r}{\xi L_r} i_{rq} + \frac{L_m}{\xi L_r L_s} u_{sq} - \frac{1}{\xi L_r} u_{rq} \\
\frac{d\Omega_r}{dt} &= -\frac{D_r}{J_r}\Omega_r + \frac{K_{opt}}{J_r}\Omega_r^2 - \frac{n_b}{J_r} T_h \\
\frac{d\Omega_g}{dt} &= -\frac{D_g}{J_g}\Omega_g + \frac{1}{J_g} T_h - \frac{1}{J_g} T_g \\
\frac{dT_h}{dt} &= \frac{1}{n_b}\left(K_{ls} - \frac{D_r D_{ls}}{J_r}\right)\Omega_r + \frac{1}{n_b}\left(\frac{D_{ls} K_{opt}}{J_r}\right)\Omega_r^2 - \frac{1}{n_b^2}\left(K_{ls} - \frac{D_g D_{ls}}{J_g}\right)\Omega_g \\
&\quad - D_{ls}\left(\frac{1}{J_r} + \frac{1}{n_b^2 J_g}\right) T_h + \frac{D_{ls}}{n_b^2 J_g} T_g \\
\frac{dT_g}{dt} &= -\frac{1}{\tau_g} T_g + \frac{1}{\tau_g} T_{g,r}
\end{aligned} \tag{9}$$

where:

D_g: the damping constants for the generator,
D_{ls}: the damping constants for the the equivalent low-speed shaft,
D_r: the damping constants for the rotor,
i_m: the magnetizing current,
J_g: the moment of inertia of the generator,
J_r: the moment of inertia of the rotor,
K_{ls}: the equivalent torsional stiffness of the low-speed shaft,
n_b: the gearbox ratio (the gearbox is considered as a lossless device for this model),
R_r: the rotor resistance,
R_s: the stator resistance,
τ_g: the time constant of the model,
V_s: the stator voltage magnitude.

For the ease of presentation, we define the following parameters for the wind energy conversion system, $p_1 = \frac{-R_s}{\xi L_s}$, $p_2 = \omega_s$, $p_3 = \frac{1-\xi}{\xi} n_p$, $p_4 = \frac{R_r L_m}{\xi L_r L_s}$, $p_5 = \frac{L_m}{\xi L_s} n_p$, $p_6 = -\frac{1}{\xi L_s}$, $p_7 = \frac{L_m}{\xi L_r L_s}$, $p_8 = -\frac{L_m}{\xi L_r} n_p$, $p_9 = -\frac{R_r}{\xi L_r}$, $p_{10} = -\frac{1}{\xi} n_p$, $p_{11} = -\frac{1}{\xi L_r}$, $p_{12} = \frac{R_s L_m}{\xi L_r L_s}$, $p_{13} = -\frac{D_r}{J_r}$, $p_{14} = \frac{K_{opt}}{J_r}$, $p_{15} = -\frac{n_b}{J_r}$, $p_{16} = -\frac{D_g}{J_g}$, $p_{17} = \frac{1}{J_g}$, $p_{18} = \frac{1}{n_b}(K_{ls} - \frac{D_r D_{ls}}{J_r})$, $p_{19} = \frac{1}{n_b}(\frac{D_{ls} K_{opt}}{J_r})$, $p_{20} = -\frac{1}{n_b^2}(K_{ls} - \frac{D_g D_{ls}}{J_g})$, $p_{21} = -D_{ls}(\frac{1}{J_r} + \frac{1}{n_b^2 J_g})$, $p_{22} = \frac{D_{ls}}{n_b^2 J_g}$, $p_{23} = -\frac{1}{\tau_g}$.

Moreover, we define the state variable vector x, which contains the states x_1–x_8, such that,

$$x = [x_1 \ x_2 \ x_3 \ x_4 \ x_5 \ x_6 \ x_7 \ x_8]^T = [i_{sd} \ i_{sq} \ i_{rd} \ i_{rq} \ \Omega_r \ \Omega_g \ T_h \ T_g]^T. \tag{10}$$

Therefore, the model of the wind energy power system in (10) can be written in compact form as follows,

$$\begin{aligned}
\dot{x}_1 &= p_1 x_1 + p_2 x_2 + p_3 x_6 x_2 + p_4 x_3 + p_5 x_4 x_6 + p_6 u_{sd} + p_7 u_{rd} \\
\dot{x}_2 &= -p_2 x_1 - p_3 x_6 x_1 + p_1 x_2 - p_5 x_6 x_3 + p_4 x_4 + p_6 u_{sq} + p_7 u_{rq} \\
\dot{x}_3 &= p_{12} x_1 + p_8 x_6 x_2 + p_9 x_3 + p_2 x_4 + p_{10} x_6 x_4 + p_7 u_{sd} + p_{11} u_{rd} \\
\dot{x}_4 &= -p_8 x_6 x_1 + p_{12} x_2 - p_2 x_3 - p_{10} x_6 x_3 + p_9 x_4 + p_7 u_{sq} + p_{11} u_{rq} \\
\dot{x}_5 &= p_{13} x_5 + p_{14} x_5^2 + p_{15} x_7 \\
\dot{x}_6 &= p_{16} x_6 + p_{17} x_7 - p_{17} x_8 \\
\dot{x}_7 &= p_{18} x_5 + p_{19} x_5^2 + p_{20} x_6 + p_{21} x_7 + p_{22} x_8 \\
\dot{x}_8 &= p_{23} x_8 - p_{23} T_{g,r}
\end{aligned} \tag{11}$$

Let the desired state vector x_d be such that $x_d = [x_{1d} \ x_{2d} \ x_{3d} \ x_{4d} \ x_{5d} \ x_{6d} \ x_{7d} \ x_{8d}]^T$, where x_{id} $(i = 1, 2, ..., 8)$ are the desired values of the states x_i $(i = 1, 2, ..., 8)$ of the power system. Since the desired states have to be an operating point of the power system, then they must satisfy the equations of the model of the wind energy power system in (12). Therefore, the desired states of the power system are governed by the following set of differential equations:

$$\dot{x}_{1d} = p_1 x_{1d} + p_2 x_{2d} + p_3 x_{6d} x_{2d} + p_4 x_{3d} + p_5 x_{4d} x_{6d} + p_6 \bar{u}_{sd} + p_7 \bar{u}_{rd} \tag{12}$$

$$\dot{x}_{2d} = -p_2 x_{1d} - p_3 x_{6d} x_{1d} + p_1 x_{2d} - p_5 x_{6d} x_{3d} + p_4 x_{4d} + p_6 \bar{u}_{sq} + p_7 \bar{u}_{rq} \tag{13}$$

$$\dot{x}_{3d} = p_{12} x_{1d} + p_8 x_{6d} x_{2d} + p_9 x_{3d} + p_2 x_{4d} + p_{10} x_{6d} x_{4d} + p_7 \bar{u}_{sd} + p_{11} \bar{u}_{rd} \tag{14}$$

$$\dot{x}_{4d} = -p_8 x_{6d} x_{1d} + p_{12} x_{2d} - p_2 x_{3d} - p_{10} x_{6d} x_{3d} + p_9 x_{4d} + p_7 \bar{u}_{sq} + p_{11} \bar{u}_{rq} \tag{15}$$

$$\dot{x}_{5d} = p_{13} x_{5d} + p_{14} x_{5d}^2 + p_{15} x_{7d} \tag{16}$$

$$\dot{x}_{6d} = p_{16} x_{6d} + p_{17} x_{7d} - p_{17} x_{8d} \tag{17}$$

$$\dot{x}_{7d} = p_{18} x_{5d} + p_{19} x_{5d}^2 + p_{20} x_{6d} + p_{21} x_{7d} + p_{22} x_{8d} \tag{18}$$

$$\dot{x}_{8d} = p_{23} x_{8d} - p_{23} \bar{T}_{g,r} \tag{19}$$

Note that $\bar{u}_{sd}$, $\bar{u}_{sq}$, $\bar{u}_{rd}$, $\bar{u}_{rq}$ and $\bar{T}_{g,r}$ in (12)–(19) represent the reference inputs of the wind energy conversion system. The computation of these reference inputs will be discussed in the next section.

Define the errors e_i $(i = 1, 2, ..., 8)$, such that:

$$\begin{aligned} e_1 &= x_1 - x_{1d} \\ e_2 &= x_2 - x_{2d} \\ e_3 &= x_3 - x_{3d} \\ e_4 &= x_4 - x_{4d} \\ e_5 &= x_5 - x_{5d} \\ e_6 &= x_6 - x_{6d} \\ e_7 &= x_7 - x_{7d} \\ e_8 &= x_8 - x_{8d} \end{aligned} \tag{20}$$

Using Equations (12)–(21), the dynamic model of the error system can be written, such that:

$$\begin{aligned} \dot{e}_1 &= p_1 e_1 + p_2 e_2 + p_3(x_6 x_2 - x_{6d} x_{2d}) + p_4 e_3 + p_5(x_4 x_6 - x_{4d} x_{6d}) + v_1 \\ \dot{e}_2 &= -p_2 e_1 - p_3(x_6 x_1 - x_{6d} x_{1d}) + p_1 e_2 - p_5(x_6 x_3 - x_{6d} x_{3d}) + p_4 e_4 + v_2 \\ \dot{e}_3 &= p_{12} e_1 + p_8(x_6 x_2 - x_{6d} x_{2d}) + p_9 e_3 + p_2 e_4 + p_{10}(x_6 x_4 - x_{6d} x_{4d}) + v_3 \\ \dot{e}_4 &= -p_8(x_6 x_1 - x_{6d} x_{1d}) + p_{12} e_2 - p_2 e_3 - p_{10}(x_6 x_3 - x_{6d} x_{3d}) + p_9 e_4 + v_4 \\ \dot{e}_5 &= p_{13} e_5 + p_{14}(x_5^2 - x_{5d}^2) + p_{15} e_7 \\ \dot{e}_6 &= p_{16} e_6 + p_{17} e_7 - p_{17} e_8 \\ \dot{e}_7 &= p_{18} e_5 + p_{19}(x_5^2 - x_{5d}^2) + p_{20} e_6 + p_{21} e_7 + p_{22} e_8 \\ \dot{e}_8 &= p_{23} e_8 + v_g \end{aligned} \tag{21}$$

where the inputs v_1, v_2, v_3, v_4 and v_g are defined, such that,

$$\begin{aligned} v_1 &= p_6(u_{sd} - \bar{u}_{sd}) + p_7(u_{rd} - \bar{u}_{rd}) \\ v_2 &= p_6(u_{sq} - \bar{u}_{sq}) + p_7(u_{rq} - \bar{u}_{rq}) \\ v_3 &= p_7(u_{sd} - \bar{u}_{sd}) + p_{11}(u_{rd} - \bar{u}_{rd}) \\ v_4 &= p_7(u_{sq} - \bar{u}_{sq}) + p_{11}(u_{rq} - \bar{u}_{rq}) \\ v_g &= -p_{23}(T_{g,r} - \bar{T}_{g,r}). \end{aligned} \tag{22}$$

After some manipulations, the error dynamics in (22) can be written as follows,

$$\dot{e}_1 = p_1 e_1 + p_2 e_2 + p_3(e_6 e_2 + x_{6d} e_2 + x_{2d} e_6) + p_4 e_3 + p_5(e_4 e_6 + x_{4d} e_6 + x_{6d} e_4) + v_1 \tag{23}$$

$$\dot{e}_2 = -p_2 e_1 - p_3(e_6 e_1 + x_{6d} e_1 + x_{1d} e_6) + p_1 e_2 - p_5(e_6 e_3 + x_{6d} e_3 + x_{3d} e_6) + p_4 e_4 + v_2 \tag{24}$$

$$\dot{e}_3 = p_{12} e_1 + p_8(e_6 e_2 + x_{6d} e_2 + x_{2d} e_6) + p_9 e_3 + p_2 e_4 + p_{10}(e_4 e_6 + x_{4d} e_6 + x_{6d} e_4) + v_3 \tag{25}$$

$$\dot{e}_4 = -p_8(e_6 e_1 + x_{6d} e_1 + x_{1d} e_6) + p_{12} e_2 - p_2 e_3 - p_{10}(e_6 e_3 + x_{6d} e_3 + x_{3d} e_6) + v_4 \tag{26}$$

$$\dot{e}_5 = p_{13} e_5 + p_{14}(e_5^2 + 2 x_{5d} e_5) + p_{15} e_7 \tag{27}$$

$$\dot{e}_6 = p_{16} e_6 + p_{17} e_7 - p_{17} e_8 \tag{28}$$

$$\dot{e}_7 = p_{18} e_5 + p_{19}(e_5^2 + 2 x_{5d} e_5) + p_{20} e_6 + p_{21} e_7 + p_{22} e_8 \tag{29}$$

$$\dot{e}_8 = p_{23} e_8 + v_g \tag{30}$$

Define the matrix M_u and the vectors u, v and $\bar{u}_r$, such that,

$$M_u = \begin{bmatrix} p_6 & p_7 & 0 & 0 & 0 \\ 0 & 0 & p_6 & p_7 & 0 \\ p_7 & p_{11} & 0 & 0 & 0 \\ 0 & 0 & p_7 & p_{11} & 0 \\ 0 & 0 & 0 & 0 & -p_{23} \end{bmatrix}, \quad u = \begin{bmatrix} u_{sd} \\ u_{rd} \\ u_{sq} \\ u_{rq} \\ T_{g,r} \end{bmatrix}, \quad v = \begin{bmatrix} v_1 \\ v_2 \\ v_3 \\ v_4 \\ v_g \end{bmatrix}, \quad \bar{u}_r = \begin{bmatrix} \bar{u}_{sd} \\ \bar{u}_{rd} \\ \bar{u}_{sq} \\ \bar{u}_{rq} \\ \bar{T}_{g,r} \end{bmatrix}. \tag{31}$$

Remark 1. *The controller* $u = \begin{bmatrix} u_{sd} & u_{rd} & u_{sq} & u_{rq} & T_{g,r} \end{bmatrix}^T$ *of the wind energy conversion system model in (12) is computed using the controller* $v = \begin{bmatrix} v_1 & v_2 & v_3 & v_4 & v_g \end{bmatrix}^T$ *and the reference inputs* $\bar{u}_{sd}$, $\bar{u}_{sq}$, $\bar{u}_{rd}$, $\bar{u}_{rq}$ *and* $\bar{T}_{g,r}$, *such that,*

$$\begin{bmatrix} u_{sd} \\ u_{rd} \\ u_{sq} \\ u_{rq} \\ T_{g,r} \end{bmatrix} = \begin{bmatrix} p_6 & p_7 & 0 & 0 & 0 \\ 0 & 0 & p_6 & p_7 & 0 \\ p_7 & p_{11} & 0 & 0 & 0 \\ 0 & 0 & p_7 & p_{11} & 0 \\ 0 & 0 & 0 & 0 & -p_{23} \end{bmatrix}^{-1} \begin{bmatrix} v_1 \\ v_2 \\ v_3 \\ v_4 \\ v_g \end{bmatrix} + \begin{bmatrix} \bar{u}_{sd} \\ \bar{u}_{rd} \\ \bar{u}_{sq} \\ \bar{u}_{rq} \\ \bar{T}_{g,r} \end{bmatrix} \tag{32}$$

Equation (32) can be written in compact form, such that,

$$u = M_u^{-1} v + \bar{u}_r. \tag{33}$$

Note that the determinant of the matrix M_u *equals* $p_{23}(p_7^2 - p_6 p_{11})^2$, *which is different from zero. Hence, the matrix* M_u *is nonsingular, and its inverse always exists.*

3. Computations of the Desired States and the Reference Inputs of the WEC System

This section deals with the computations of the values of the desired states of the wind energy conversion system, as well as the values of the reference inputs of the system.

3.1. Computation of the Desired States of the WEC System

The flux linkages of the stator and the rotor of the generator can be expressed as,

$$\psi_{sd} = L_s i_{sd} + L_m i_{rd} \tag{34}$$
$$\psi_{sq} = L_s i_{sq} + L_m i_{rq} \tag{35}$$
$$\psi_{rd} = L_r i_{rd} + L_m i_{sd} \tag{36}$$
$$\psi_{rq} = L_r i_{rq} + L_m i_{sq} \tag{37}$$

where ψ_{sd} is the stator d-axis flux linkage and ψ_{sq} is the stator q-axis flux linkage. The flux ψ_{rd} is the rotor d-axis flux linkage, and ψ_{rq} is the rotor q-axis flux linkage.

The stator active power, P_s, and the stator reactive power, Q_s, can be expressed as follows,

$$P_s = \frac{3}{2}(u_{sd} i_{sd} + u_{sq} i_{sq}) \tag{38}$$
$$Q_s = \frac{3}{2}(u_{sq} i_{sd} - u_{sd} i_{sq}) \tag{39}$$

where i_{sd} and i_{sq} are the stator currents; u_{sd} and u_{sq} are the stator voltages.

In the stator voltage oriented reference frame, the q-axis is aligned with the supply voltage V_s; then, the reference inputs $\bar{u}_{sd}$ and $\bar{u}_{sq}$ are such that $\bar{u}_{sd} = 0$ and $\bar{u}_{sq} = V_s$.

Using Equations (38)–(39), the desired stator active and reactive powers can be written as follows,

$$P_{s_d} = \frac{3}{2}(\bar{u}_{sd}x_{1d} + \bar{u}_{sq}x_{2d}) = \frac{3}{2}x_{2d}V_s \quad (40)$$

$$Q_{s_d} = \frac{3}{2}(\bar{u}_{sq}x_{1d} - \bar{u}_{sd}x_{2d}) = \frac{3}{2}x_{1d}V_s \quad (41)$$

where x_{1d} is the desired value of i_{sd} and x_{2d} is the desired value of i_{sq}.

Moreover, the stator flux ψ_s is set to be aligned with the d-axis; hence, the stator d-axis and q-axis flux linkages are such that $\psi_{sd} = \psi_s = V_s/\omega_s$ and $\psi_{sq} = 0$. In addition, we choose to set the desired stator active power P_{s_d} to be equal to the maximum power that can be captured from the wind and the desired stator reactive power Q_{s_d} to be zero, then $P_{s_d} = P_{m(\max)}$ and $Q_{s_d} = 0$.

Remark 2. *Note that the desired reactive power is selected to ensure a unity power factor.*

Hence, the desired states x_{1d}, x_{2d}, x_{3d}, x_{4d}, x_{5d}, x_{6d}, x_{7d} and x_{8d} are computed as follows.

At first, using Equations (40) and (41), we can compute x_{1d} and x_{2d} as follows,

$$x_{1d} = \frac{2}{3}\frac{Q_{sd}}{V_s} = 0 \quad (42)$$

$$x_{2d} = \frac{2}{3}\frac{P_{sd}}{V_s} = \frac{2}{3}\frac{P_{m(max)}}{V_s}. \quad (43)$$

Then, using Equations (34) and (35) with $\psi_{sd} = \psi_s = V_s/\omega_s$ and $\psi_{sq} = 0$, we can compute x_{3d} and x_{4d}, which are the desired values of i_{rd} and i_{rq}, as follows,

$$x_{3d} = \frac{1}{L_m}\frac{V_s}{\omega_s} \quad (44)$$

$$x_{4d} = -\frac{2}{3}\frac{L_s}{L_m}\frac{P_{m(max)}}{V_s}. \quad (45)$$

Furthermore, the desired value of generator torque x_{8d} is chosen to provide an appropriate opposing torque. Using Equations (2) and (4), x_{8d} can be written as follows,

$$x_{8d} = -\frac{1}{2}n_b\rho\pi R^3 C_{p(max)}V^2/\lambda_{opt}. \quad (46)$$

Finally, the remaining desired states x_{5d}, x_{6d} and x_{7d}, which are the desired values of Ω_r, Ω_g, T_h, are determined by solving the ordinary differential Equations (16)–(18). Recall that these equations are as follows,

$$\dot{x}_{5d} = p_{13}x_{5d} + p_{14}x_{5d}^2 + p_{15}x_{7d} \quad (47)$$

$$\dot{x}_{6d} = p_{16}x_{6d} + p_{17}x_{7d} - p_{17}x_{8d} \quad (48)$$

$$\dot{x}_{7d} = p_{18}x_{5d} + p_{19}x_{5d}^2 + p_{20}x_{6d} + p_{21}x_{7d} + p_{22}x_{8d} \quad (49)$$

3.2. Computation of the Reference Inputs of the WEC System

Recall that in the stator voltage-oriented reference frame, it is assumed that the q-axis is aligned with the supply voltage V_s. Hence, the reference inputs $\bar{u}_{sd}$ and $\bar{u}_{sq}$ are such that $\bar{u}_{sd} = 0$ and $\bar{u}_{sq} = V_s$. On the other hand, the reference inputs $\bar{u}_{rd}$, $\bar{u}_{rq}$ and $\bar{T}_{g,r}$ are computed as follows. First, we define the terms c_1, c_2, c_3, c_4 and c_5, such that,

$$c_1 = p_1x_{1d} + p_2x_{2d} + p_3x_{6d}x_{2d} + p_4x_{3d} + p_5x_{4d}x_{6d} \quad (50)$$

$$c_2 = -p_2x_{1d} - p_3x_{6d}x_{1d} + p_1x_{2d} - p_5x_{6d}x_{3d} + p_4x_{4d} \quad (51)$$

$$c_3 = p_{23}x_{8d} \quad (52)$$

$$c_4 = \dot{x}_{2d} = C_{p(\max)}(\lambda_{opt}, \beta)\rho\pi R^2V^2\dot{V} \quad (53)$$

$$c_5 = \dot{x}_{8d} = -\frac{n_b}{\lambda_{opt}}C_{p(\max)}(\lambda_{opt}, \beta)\rho\pi R^2V^2\dot{V} \quad (54)$$

where $\dot{V}$ represents the derivative with respect to time of the wind speed model.

Then, using Equations (12), (13) and (19), the reference inputs are obtained, such that,

$$\begin{aligned}
\bar{u}_{sd} &= 0 && (55)\\
\bar{u}_{rd} &= -\frac{1}{p_7}c_1 && (56)\\
\bar{u}_{sq} &= V_s && (57)\\
\bar{u}_{rq} &= \frac{1}{p_7}(c_4 - c_2 - p_6 V_s) && (58)\\
\bar{T}_{g,r} &= \frac{1}{p_{23}}(p_{23}x_{8d} - c_5) && (59)
\end{aligned}$$

4. A Feedback Linearization Controller for the Wind Energy Conversion System

This section deals with the design of a feedback linearization control law for the wind energy conversion system represented by the nonlinear system of odes given by (12).

We start with defining the variables z_1, z_2 and z_3, such that,

$$\begin{aligned}
z_1 &= e_5 && (60)\\
z_2 &= p_{13}e_5 + p_{14}(e_5^2 + 2x_{5d}e_5) + p_{15}e_7 && (61)\\
z_3 &= (p_{13} + 2p_{14}e_5 + 2p_{14}x_{5d})[p_{13}e_5 + p_{14}(e_5^2 + 2x_{5d}e_5) + p_{15}e_7]\\
&\quad +2p_{14}\dot{x}_{5d}e_5 + p_{15}[p_{18}e_5 + p_{19}(e_5^2 + 2x_{5d}e_5) + p_{20}e_6 + p_{21}e_7 + p_{22}e_8]. && (62)
\end{aligned}$$

Furthermore, define the functions f_1 and f_2, such that:

$$\begin{aligned}
f_1 &= (p_{13} + 2p_{14}e_5 + 2p_{14}x_{5d})[p_{13}e_5 + p_{14}(e_5^2 + 2x_{5d}e_5) + p_{15}e_7]\\
&\quad +2p_{14}\dot{x}_{5d}e_5 + p_{15}[p_{18}e_5 + p_{19}(e_5^2 + 2x_{5d}e_5) + p_{20}e_6 + p_{21}e_7] && (63)\\
f_2 &= 2p_{14}(p_{13}e_5 + p_{14}(e_5^2 + 2x_{5d}e_5) + p_{15}e_7 + 2\dot{x}_{5d})z_2\\
&\quad +(p_{13} + 2p_{14}e_5 + 2p_{14}x_{5d})z_3 + 2p_{14}\ddot{x}_{5d}e_5\\
&\quad +p_{15}[p_{18}z_2 + 2p_{19}(e_5 + x_{5d})z_2 + 2p_{19}\dot{x}_{5d}e_5] + p_{15}p_{20}(p_{16}e_6 + p_{17}e_7 - p_{17}e_8)\\
&\quad +p_{15}p_{21}(p_{18}e_5 + p_{19}(e_5^2 + 2x_{5d}e_5) + p_{20}e_6 + p_{21}e_7 + p_{22}e_8) && (64)
\end{aligned}$$

Let the control parameters α_1, α_2, α_3 and α_4 be positive scalars and choose the parameters β_1, β_2 and β_3 to be positive scalars, such that the polynomial $P_1(s) = s^3 + \beta_3 s^2 + \beta_2 s + \beta_1$ is Hurwitz.

The following proposition gives the feedback linearization controller.

Proposition 1. *The feedback linearization controller,*

$$u = M_u^{-1}v + \bar{u}_r \quad (65)$$

with M_u and $\bar{u}_r$ given by (31) and (55)–(59) and $v = [v_1 \quad v_1 \quad v_1 \quad v_1 \quad v_g]^T$, such that,

$$\begin{aligned}
v_1 &= -p_2e_2 - p_3(e_6e_2 + x_{6d}e_2 + x_{2d}e_6) - p_4e_3 - p_5(e_4e_6 + x_{4d}e_6 + x_{6d}e_4) - \alpha_1e_1 && (66)\\
v_2 &= p_2e_1 + p_3(e_6e_1 + x_{6d}e_1 + x_{1d}e_6) + p_5(e_6e_3 + x_{6d}e_3 + x_{3d}e_6) - p_4e_4 - \alpha_2e_2 && (67)\\
v_3 &= -p_{12}e_1 - p_8(e_6e_2 + x_{6d}e_2 + x_{2d}e_6) - p_2e_4 - p_{10}(e_4e_6 + x_{4d}e_6 + x_{6d}e_4) - \alpha_3e_3 && (68)\\
v_4 &= p_8(e_6e_1 + x_{6d}e_1 + x_{1d}e_6) - p_{12}e_2 + p_2e_3 + p_{10}(e_6e_3 + x_{6d}e_3 + x_{3d}e_6) - \alpha_4e_4 && (69)\\
v_g &= \frac{1}{p_{15}p_{22}}(-f_2 - p_{15}p_{22}p_{23}e_8 - \beta_1z_1 - \beta_2z_2 - \beta_3z_3) && (70)
\end{aligned}$$

when applied to the model of the wind energy power system given by (12) guarantees the asymptotic convergence of the states of the system to their desired values.

Note that the block diagram representation of the DFIG-based WEC system with the proposed controller is depicted in Figure 3.

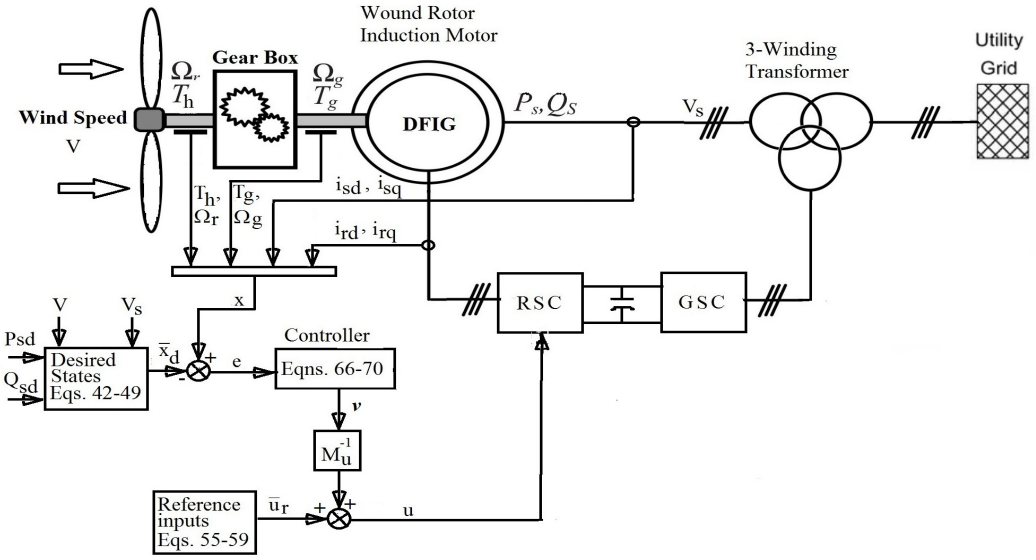

Figure 3. A block diagram representation of the variable speed DFIG-based wind energy conversion system with the proposed controller. GSC, grid side converter.

Proof. Applying the controllers given by (66)–(69) to the first four differential equations of the error system given by (23)–(26), we obtain:

$$\begin{aligned} \dot{e}_1 &= -(\alpha_1 - p_1)e_1 \\ \dot{e}_2 &= -(\alpha_2 - p_1)e_2 \\ \dot{e}_3 &= -(\alpha_3 - p_9)e_3 \\ \dot{e}_4 &= -\alpha_4 e_4. \end{aligned} \tag{71}$$

Because the α_i's $(i = 1, ..., 4)$ are chosen to be positive scalars and since the parameters $p_1 = -\frac{R_s}{\zeta L_s}$ and $p_9 = -\frac{R_r}{\zeta L_r}$ are negative, then it can be concluded from the system of odes in (72) that the errors e_1, e_2, e_3 and e_4 asymptotically converge to zero as t tends to infinity.

The second part of the proof involves proving the asymptotic convergence to zero of the errors e_5, e_6, e_7 and e_8. Taking the time derivative of the variables z_1, z_2 and z_3 defined in Equations (60)–(62) and using the equations of the error system given by (23)–(30), we obtain:

$$\begin{aligned} \dot{z}_1 &= z_2 \\ \dot{z}_2 &= z_3 \\ \dot{z}_3 &= f_2 + p_{15}p_{22}(p_{23}e_8 + v_g) \end{aligned} \tag{72}$$

The application of the controller v_g in (70) to the system of odes in (73), yields,

$$\begin{aligned} \dot{z}_1 &= z_2 \\ \dot{z}_2 &= z_3 \\ \dot{z}_3 &= -\beta_1 z_1 - \beta_2 z_2 - \beta_3 z_3 \end{aligned} \tag{73}$$

The above system can be written in compact form, such that:

$$\dot{z} = M_z z \tag{74}$$

with the matrix M_z and the vector z being such that,

$$M_z = \begin{bmatrix} 0 & 1 & 0 \\ 0 & 0 & 1 \\ -\beta_1 & -\beta_2 & -\beta_3 \end{bmatrix}, \quad z = \begin{bmatrix} z_1 \\ z_2 \\ z_3 \end{bmatrix}.$$

Since β_1, β_2 and β_3 are positive scalars, such that the polynomial $P_1(s) = s^3 + \beta_3 s^2 + \beta_2 s + \beta_1$ is Hurwitz, then the matrix M_z is a stable matrix (i.e., its eigenvalues are located in the left half of the s-plane). The solution of the Equation (74) is $z(t) = exp(M_z t)z(0)$, where $z(0)$ is the value of $z(t)$ when $t = 0$. Therefore, the asymptotic convergence of z_1, z_2 and z_3 to zero as t tends to infinity is guaranteed because M_z is a stable matrix.

The zero dynamics [44] is defined as the internal dynamics of the system when the output is kept identically zero by a suitable input function. For the third order system given by (73), the zero dynamics is analyzed by studying Equations (27)–(30) when $z_1 = 0$, $z_2 = 0$ and $z_3 = 0$.

Using Equations (60) and (61), it is clear that the asymptotic convergence of z_1 and z_2 to zero implies the asymptotic convergence of e_5 and e_7 to zero as t tends to infinity.

Moreover, since z_1, z_2, z_3, e_5 and e_7 converge to zero as t tends to infinity, then the equation given by (62) yields,

$$e_8 = -\frac{p_{20}}{p_{22}} e_6. \tag{75}$$

As t tends to infinity, the differential Equation (28) of the error system given by (23)–(30), which represents the zero dynamics of the system, reduces to,

$$\begin{aligned} \dot{e}_6 &= p_{16} e_6 - p_{17} e_8 \\ &= (p_{16} + \frac{p_{17} p_{20}}{p_{22}}) e_6 = a_e e_6. \end{aligned} \tag{76}$$

The constant $a_e = p_{16} + \frac{p_{17} p_{20}}{p_{22}}$ in (76) is such that,

$$\begin{aligned} a_e &= p_{16} + \frac{p_{17} p_{20}}{p_{22}} \\ &= -\frac{D_g}{J_g} - \frac{1}{J_g} \frac{1}{n_b^2} (K_{ls} - \frac{D_g D_{ls}}{J_g}) \frac{n_b^2 J_g}{D_{ls}} \\ &= -\frac{D_g}{J_g} - (\frac{K_{ls}}{D_{ls}} - \frac{D_g}{J_g}) = -\frac{K_{ls}}{D_{ls}}. \end{aligned} \tag{77}$$

Therefore, since $a_e = -\frac{K_{ls}}{D_{ls}}$ is always negative, Equation (76) guarantees the asymptotic convergence of the error e_6 to zero as t tends to infinity. Moreover, Equation (75) implies the asymptotic convergence of the error e_8 to zero as t tends to infinity.

The asymptotic convergence to zero of the errors e_i $(i = 1, ..., 8)$ as t tends to infinity implies the asymptotic convergence of the states of the wind energy power system given by (12) to their desired values as t tends to infinity. □

5. Simulation Results of the Controlled Wind Energy Power System

The performance of the wind energy conversion system controlled using the proposed feedback linearization controller was simulated using the MATLAB software. The parameters of the system used for the simulation studies are given in Table 1.

Table 1. The parameters of the DFIG-based wind turbine power system.

Parameter	Value
Rated power	1.5 MW
Rated apparent power	1.5 MVA
Rated voltage (line to line)	575 v
Frequency/angular speed	$2\pi 60$ rad/s
Nominal system frequency	60 Hz
Stator resistance	0.0014 Ω
Stator leakage inductance	89.98 mH
Rotor resistance	0.99187 mΩ
Rotor leakage inductance	82.088 mH
Magnetizing inductance	1.526 mH
Inertia of the generator	53.036 kg·m^2
Pole pairs	3
Wind turbine with a rotor diameter	70 m
Air density	0.55 kg/m^3
Cut-in wind speed	4 m/s
Cut-out wind speed	25 m/s
Rated wind speed	12 m/s
Rated rotor speed	19.7 rpm
Drive-train torsion damper	1.0×10^7 Nm/s
Drive-train torsion spring	5.6×10^9 Nm/rad
Gearbox ratio	75.7098
Inertia of the rotor	34.6×10^3 kg·m^2

The wind speed model used for simulation purposes is given by the following formula:

$$\begin{aligned} V &= 12 + 0.55[\sin(0.0625w) - 0.875\sin(0.1875w) + 0.75\sin(0.3125w) \\ &- 0.625\sin(0.625w) + 0.5\sin(1.875w) + 0.25\sin(3.125w) + 0.125\sin(6.25w)] \end{aligned} \quad (78)$$

with $w = \frac{2\pi}{10}t$. The wind speed profile versus time generated using Equation (78) is depicted in Figure 4.

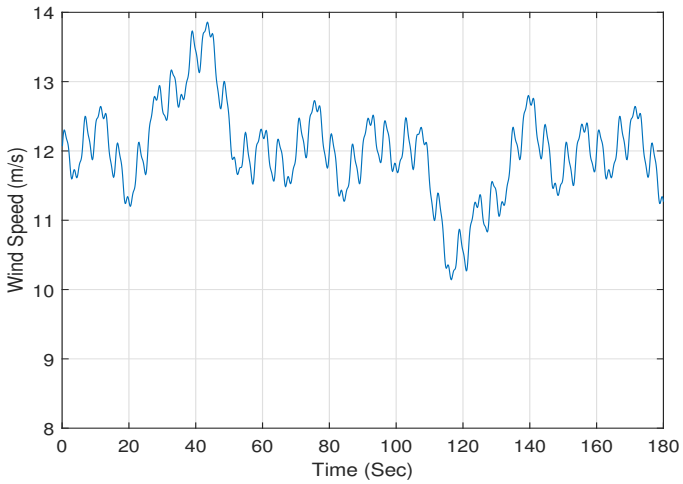

Figure 4. The wind speed profile versus time.

The wind energy conversion system was modeled using Equation (12) and controlled using the proposed feedback linearization control scheme given by Equations (65)–(70). The desired values of the states of the wind energy conversion system are obtained using Equations (42)–(49). The gains of the controller are taken to be: $\alpha_1 = 1e4$, $\alpha_2 = 3e5$, $\alpha_3 = 2e6$, $\alpha_4 = 3.5e8$, $\beta_1 = 3.15e10$, $\beta_2 = 6.35e8$ and $\beta_3 = 9.7e4$.

5.1. Simulation Studies of the WEC System When Using the Nominal Parameters of the System

The simulation results of the controlled system when using the nominal parameters are presented in Figures 5–13. Figure 5 shows the trajectory of the rotor speed Ω_r versus time, and Figure 6 depicts the trajectory of the generator speed Ω_g versus time. The high speed shaft torque and the generator torque versus time are shown in Figures 7 and 8. The errors between the actual and the desired values of the eight states of the system are shown in in Figures 9 and 10. Figure 9 shows the errors in the electrical state variables of the system versus time. It is clear from this figure that the errors e_1, e_3 and e_4 converge to zero. However, the error e_2 shows some fluctuations around zero; these fluctuations are due to the fact that e_2, which is equal to $x_2 - x_{2d}$, where x_{2d} is proportional to V^3 (V is the speed of the wind). Figure 10 shows the errors of the mechanical states variables of the system. It is clear from this figure that the errors e_5 and e_6 converge to zero. However, the errors e_7 and e_8 show some fluctuations around zero; these fluctuations are due to the fact that their desired values are dependent on the wind speed. Note that the average value of the generated torque $T_g = x_8$ is about $-2.5e7$ Nm. Therefore, it can be concluded that the states of the wind energy power system track the desired states. Figures 11 and 12 present the trajectories of the stator active and reactive powers P_s and Q_s versus time. The average of the stator active power P_s is about -0.6 MW. The average of the stator reactive power Q_s is about -0.002 MVAR. Figure 13 depicts the power coefficient C_p versus time; it is clear that the maximum value of the power coefficient is achieved when $C_{p(\max)} \approx 0.48$. It is clear from these figures that all of the closed loop system signals are bounded and that all of the states of the power system converge to their desired values.

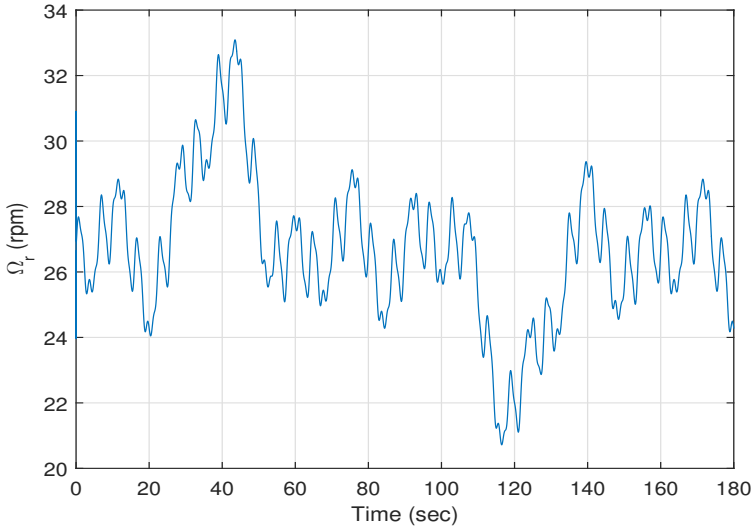

Figure 5. The turbine rotational speed on the low-speed side of the gearbox, Ω_r, versus time.

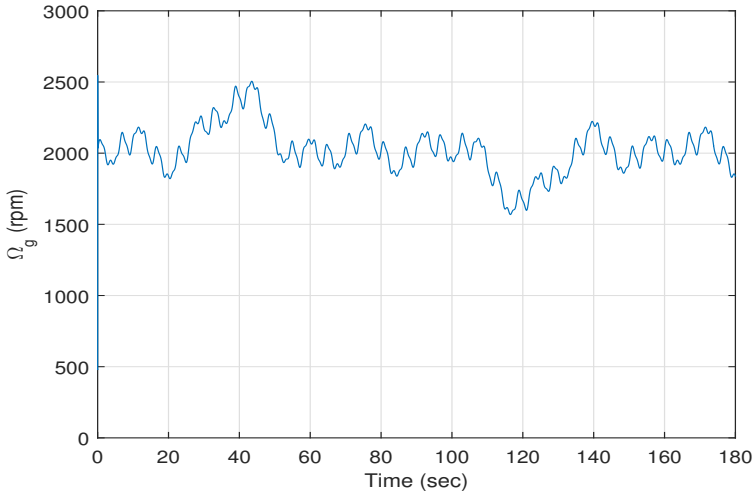

Figure 6. The mechanical generator speed Ω_g versus time.

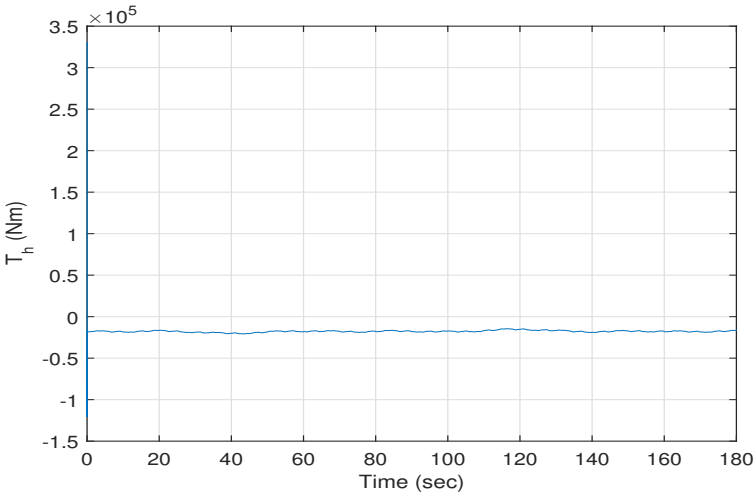

Figure 7. The high-speed shaft torque T_h versus time.

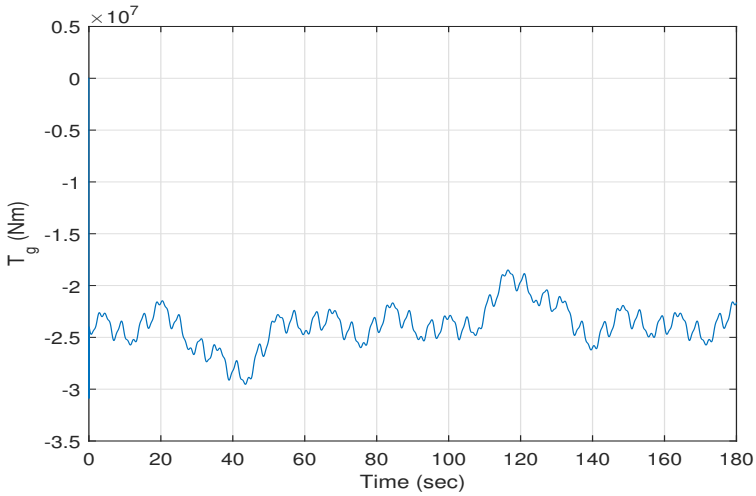

Figure 8. The generator torque T_g versus time.

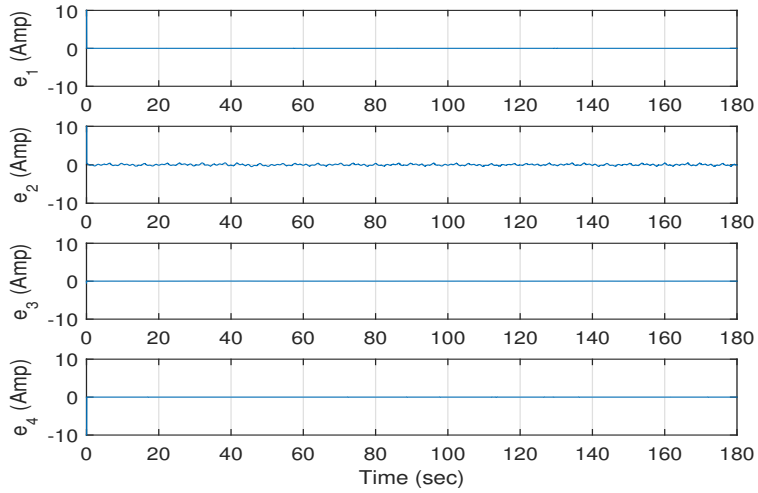

Figure 9. The errors e_1, e_2, e_3, e_4 of the electrical state variables of the WEC system versus time.

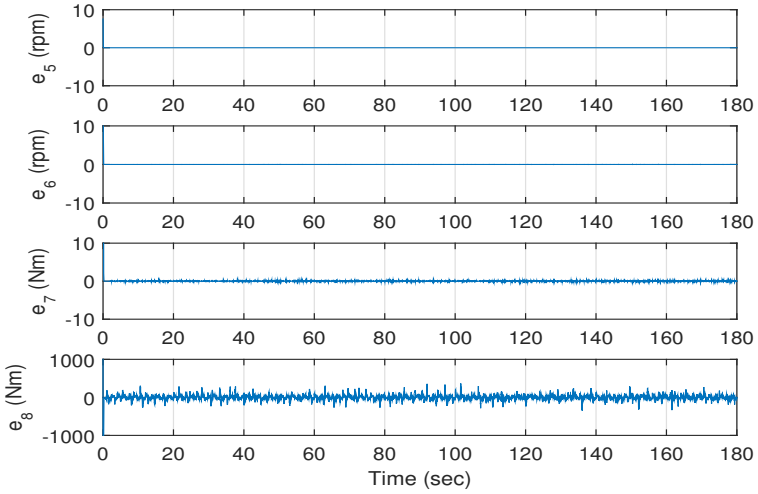

Figure 10. The errors e_5, e_6, e_7, e_8 of the mechanical state variables of the WEC system versus time.

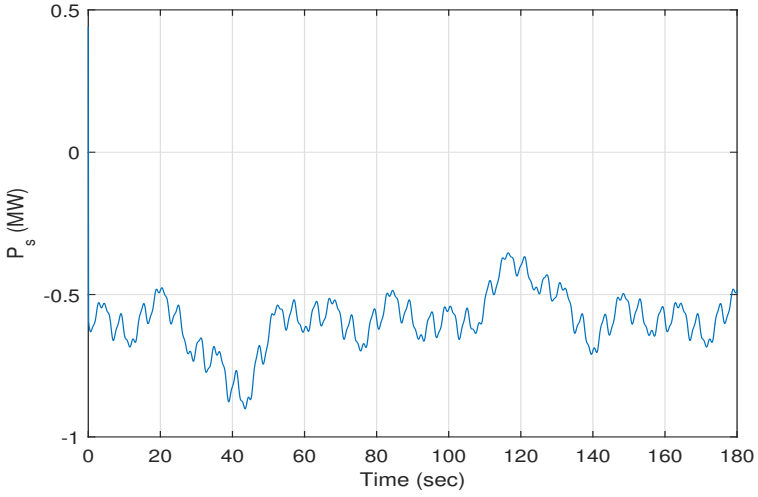

Figure 11. The stator active power P_s versus time.

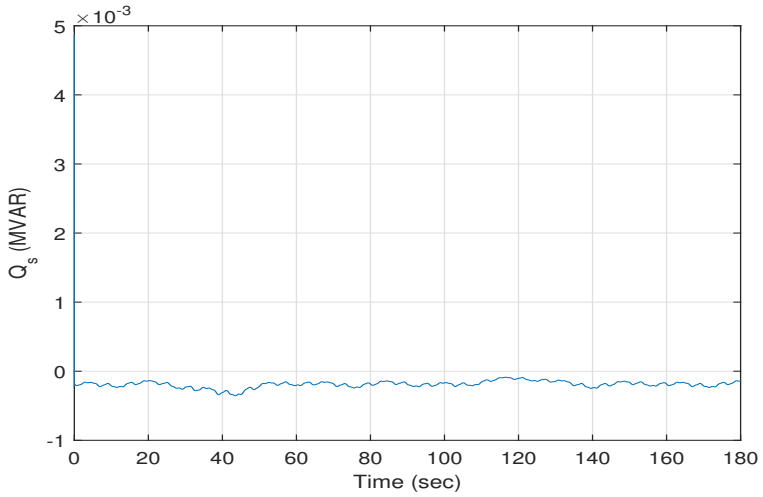

Figure 12. The stator reactive power Q_s versus time.

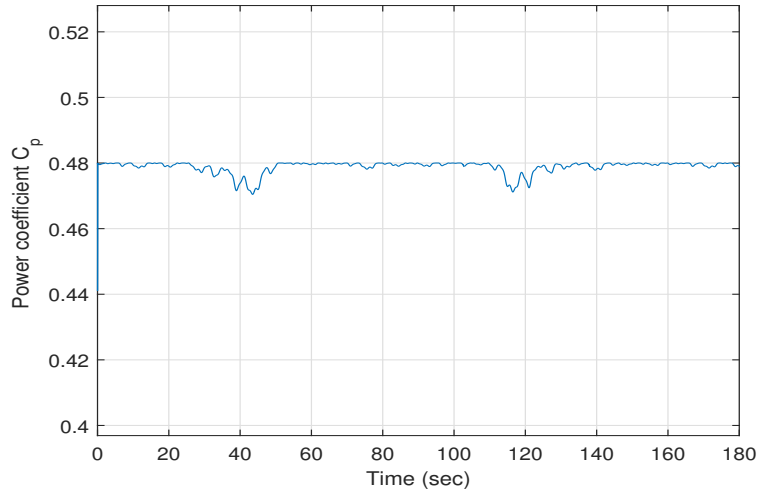

Figure 13. The power Coefficient C_p versus time.

Therefore, it can be concluded that the simulation results indicate that the wind energy conversion system controlled using the proposed feedback linearization controller shows good performance.

5.2. Robustness of the Proposed Control Scheme

Simulation studies were carried out to investigate the robustness of the proposed control scheme to changes in some of the parameters of the wind energy conversion system. At first, the effects of the changes in the stator resistance R_s, the rotor resistance R_r and the rotor inductance L_r are investigated. We simulated the performance of the closed loop system when the stator resistance R_s, the rotor resistance R_r and the rotor inductance L_r are increased by 30% of their nominal values. The responses of the system are not shown because of space limitations. However, the steady state performance of the system with the changed parameters is very similar to the steady state performance of the system with the nominal parameters. Hence, the change in some of the electrical parameters of the system did not affect the steady state performance of the system.

In addition, simulation studies were carried out to investigate the robustness of the proposed control scheme to changes in some of the electrical and some of the mechanical parameters of the wind energy conversion system. The effects of the changes in the stator resistance R_s, the rotor resistance R_r, the rotor inductance L_r, the moment of inertia of the rotor J_r and the moment of inertia of the generator J_g are investigated. Figures 14–22 show the system responses when the stator resistance

R_s, the rotor resistance R_r and the rotor inductance L_r are increased by 30%; and when the moment of inertia of the rotor J_r and the moment of inertia of the generator J_g are increased by 15% of their nominal values. Figures 14 and 15 show the rotor and the generator speed responses versus time. The high speed shaft torque and the generator torque versus time are shown in Figures 16 and 17. The errors between the actual and the desired values of the eight states of the system are shown in in Figures 18 and 19. Figure 18 shows the errors of the electrical state variables of the system versus time. It is clear from this figure that the errors e_1, e_3 and e_4 converge to zero. However, the error e_2 shows some fluctuations around zero. Figure 19 shows the errors of the mechanical states variables of the system. It is clear from this figure that the error e_5 converges to zero. However, the errors e_6, e_7 and e_8 show some fluctuations around zero. Note that in this case, the error e_7 fluctuates between -10 and 10 Nm. The error e_8 fluctuates between $-5e3$ and $5e3$ Nm. The fluctuations in the error e_8 seems to be high. However, it should be kept in mind that the average value of T_g is a bout $-2.5e7$ Nm. Even though the error is high in absolute value, it represents less than one percent of the value of T_g. Figures 20 and 21 depict the stator active and reactive powers versus time. Figure 22 depicts the power coefficient C_p. In this case, the reader can see the differences in the steady state performances of the system with the nominal parameters and the system with the changed parameters.

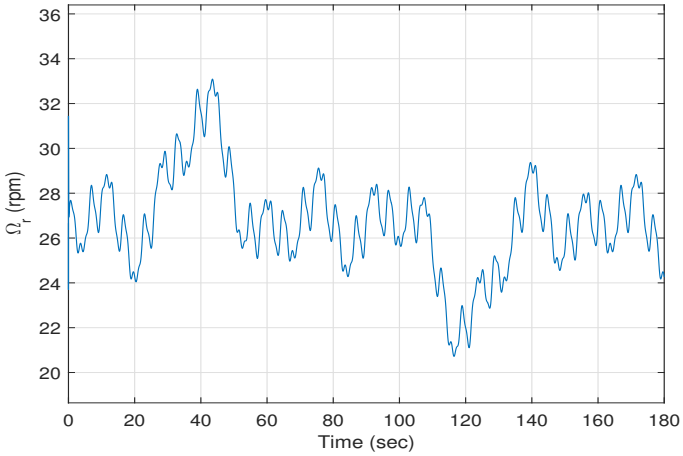

Figure 14. The turbine rotational speed on the low-speed side of the gearbox, Ω_r, versus time when R_s, R_L, L_r, J_r and J_g are different from their nominal values.

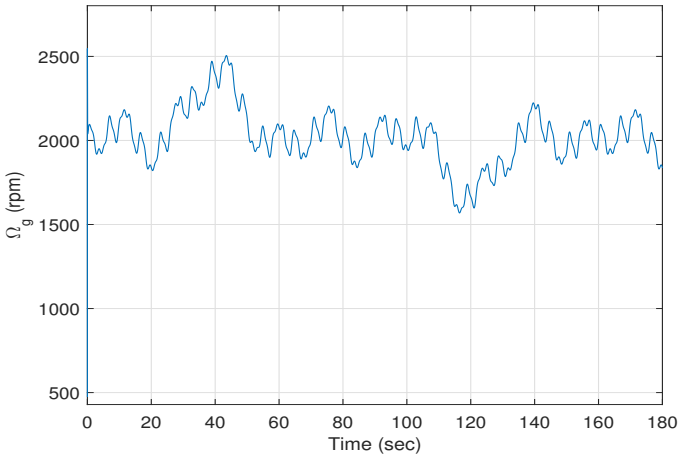

Figure 15. The mechanical generator speed Ω_g versus time when R_s, R_L, L_r, J_r and J_g are different from their nominal values.

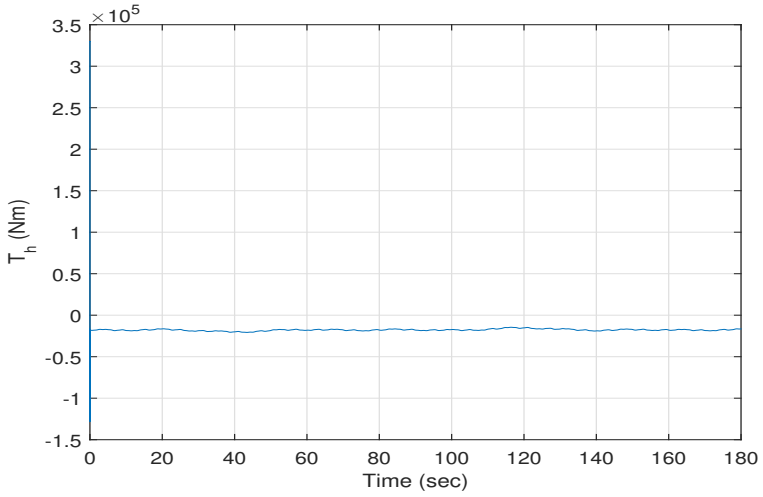

Figure 16. The high-speed shaft torque T_h versus time when R_s, R_L, L_r, J_r and J_g are different from their nominal values.

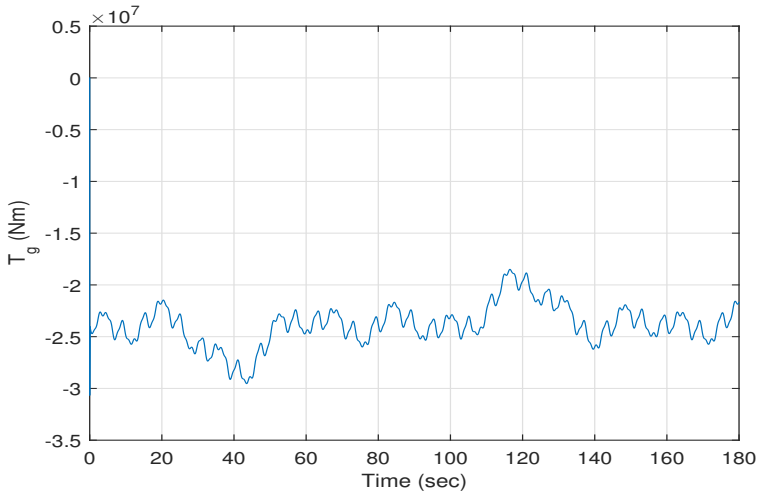

Figure 17. The generator torque T_g versus time when R_s, R_L, L_r, J_r and J_g are different from their nominal values.

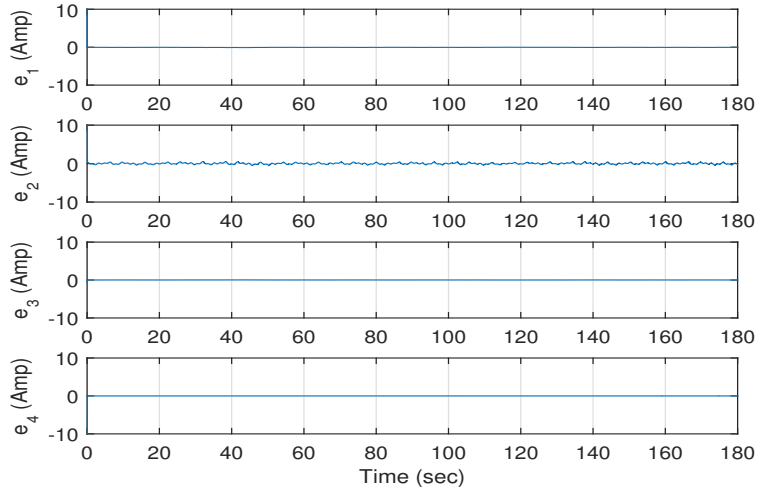

Figure 18. The errors e_1, e_2, e_3, e_4 of the electrical state variables of the WEC system versus time when R_s, R_L, L_r, J_r and J_g are different from their nominal values.

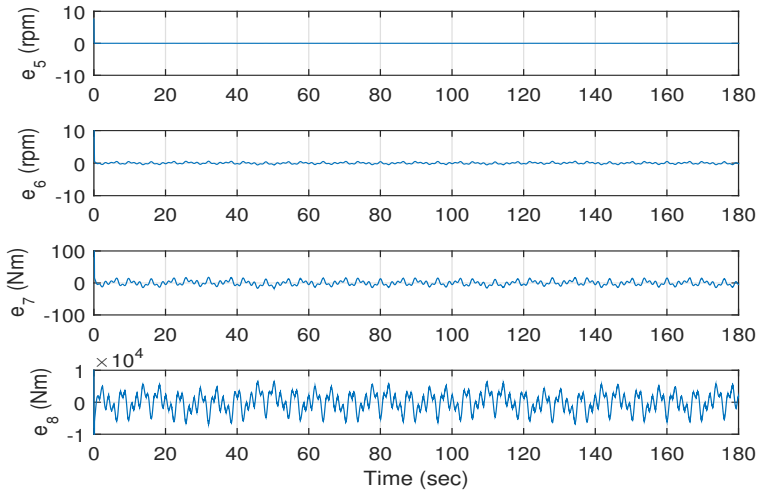

Figure 19. The errors e_5, e_6, e_7, e_8 of the mechanical state variables of the WEC system versus time when R_s, R_L, L_r, J_r and J_g are different from their nominal values.

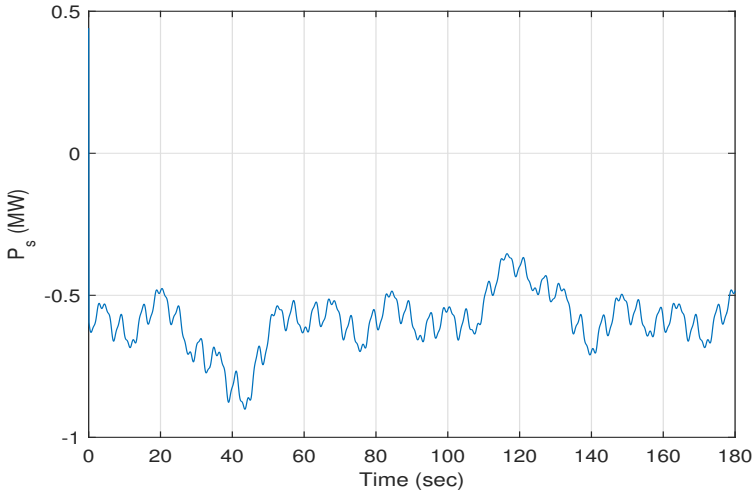

Figure 20. The stator active power P_s versus time when R_s, R_L, L_r, J_r and J_g are different from their nominal values.

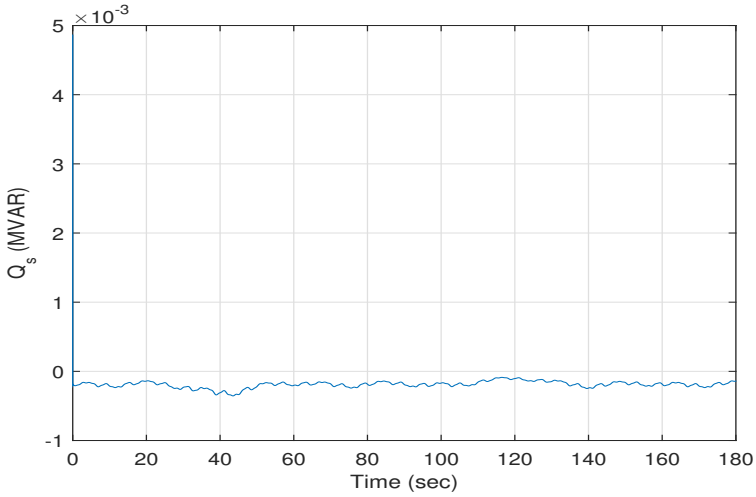

Figure 21. The stator reactive power Q_s versus time when R_s, R_L, L_r, J_r and J_g are different from their nominal values.

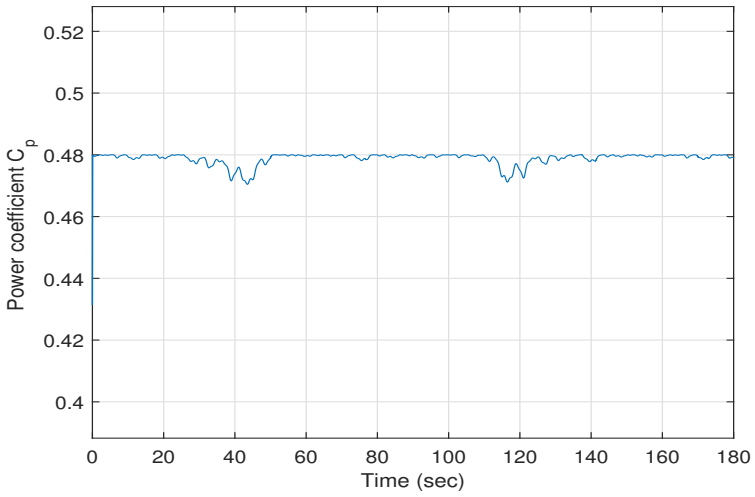

Figure 22. The power Coefficient C_p versus time when R_s, R_L, L_r, J_r and J_g are different from their nominal values.

Hence, it can be concluded that the simulation results show that the proposed controller is robust to changes in some of the electrical parameters of the wind turbine conversion system. However, the simulation results indicate that the proposed controller is sensitive to changes in some parameters of the mechanical system.

6. Conclusions

In this paper, the control of a DFIG-based wind energy power system is investigated. The power system is modeled using a system of eight nonlinear ordinary differential equations. The proposed controller is based on the feedback linearization technique. It is proven that the control scheme guarantees the asymptotic convergence of the states of the power system to their desired values. Simulation results are presented and discussed to show the effectiveness of the proposed scheme. In addition, the effects of the change of some of the parameters of the power system are studied through simulations.

Future work will address the design of other types of controllers, such as observer-based controllers and sliding mode controllers for DFIG-based wind energy power systems.

Acknowledgments: The authors would like to thank Kuwait University for covering the costs to publish this paper in open access.

Author Contributions: The first two authors contributed equally to this work. The third author contributed to the simulations of the performance of the system. All authors approved the final manuscript.

Conflicts of Interest: The authors declare no conflict of interest.

References

1. Global Wind Energy Council. 2014. Available online: http://www.gwec.net/publications/global-wind-report-2 (accessed on 14 June 2016).
2. Ling, Y.; Wu, G.; Cai, X. Comparison of wind turbine efficiency in maximum power extraction of wind turbines with doubly fed induction generator. *Prz. Elektrotech. Electr. Rev.* **2012**, *5*, 157–163.
3. Arturo Soriano, L.; Yu, W.; Rubio, J.D. Modeling and control of wind turbine. *Math. Probl. Eng.* **2013**, *2013*, 982597.
4. Haris, D.A.; Sedighizadeh, M. Nonlinear Model Identification and Adaptive Control Of Variable Speed Wind Turbine Using Recurrent Neural Network. *Int. J. Technol. Phys. Probl. Eng.* **2014**, *6*, 29–37.
5. Ghasemi, S.; Tabesh, A.; Askari-Marnani, J. Application of fractional calculus theory to robust controller design for wind turbine generators. *IEEE Trans. Energy Convers.* **2014**, *29*, 780–787.

6. Beltran, B.; Ahmed-Ali, T.; Benbouzid, M.E. Sliding mode power control of variable-speed wind energy conversion systems. *IEEE Trans. Energy Convers.* **2008**, *23*, 551–558.
7. Kairous, D.; Wamkeue, R.; Belmadani, B. Advanced control of variable speed wind energy conversion system with DFIG. In Proceedings of the 2010 IEEE 9th International Conference on the Environment and Electrical Engineering (EEEIC), Prague, Czech Republic, 16–19 May 2010; pp. 41–44.
8. Zhang, X.; Wang, Y. Robust Fuzzy Control for Doubly Fed Wind Power Systems with Variable Speed Based on Variable Structure Control Technique. *Math. Probl. Eng.* **2014**, 2014, 750101.
9. Tremblay, E.; Atayde, S.; Chandra, A. Comparative study of control strategies for the doubly fed induction generator in wind energy conversion systems: A DSP-based implementation approach. *IEEE Trans. Sustain. Energy* **2011**, *2*, 288–299.
10. Chen, Z.; Guerrero, J.M.; Blaabjerg, F. A review of the state of the art of power electronics for wind turbines. *IEEE Trans. Power Electron.* **2009**, *24*, 1859–1875.
11. Kayikci, M.; Milanovic, JV. Reactive power control strategies for DFIG-based plants. *IEEE Trans. Energy Convers.* **2007**, *22*, 389–396.
12. Xiang, D.; Ran, L.; Tavner, P.J.; Yang, S. Control of a doubly fed induction generator in a wind turbine during grid fault ride-through. *IEEE Trans. Energy Convers.* **2006**, *21*, 652–662.
13. Carrasco, J.M.; Franquelo, L.G.; Bialasiewicz, J.T.; Galván, E.; Guisado, R.C.; Prats, M.Á.; León, J.I.; Moreno-Alfonso, N. Power-electronic systems for the grid integration of renewable energy sources: A survey. *IEEE Trans. Ind. Electron.* **2006**, *53*, 1002–1016.
14. Cheng, M.; Zhu, Y. The state of the art of wind energy conversion systems and technologies: A review. *Energy Convers. Manag.* **2014**, *88*, 332–347.
15. Barambones, O. Sliding Mode Control Strategy for Wind Turbine Power Maximization. *Energies* **2012**, *5*, 2310–2330.
16. Chen, J.; Jiang, L.; Yao, W.; Wu, Q.H. Perturbation estimation based nonlinear adaptive control of a full-rated converter wind turbine for fault ride-through capability enhancement. *IEEE Trans. Power Syst.* **2014**, *29*, 2733–2743.
17. Ren, M.; Zhang, J.; Tian, Y.; Hou, G. A neural network controller for variable-speed variable-pitch wind energy conversion systems using generalized minimum entropy criterion. *Math. Probl. Eng.* **2014**, *2014*, 412027.
18. Yao, X.; Su, X.; Tian, L. Wind turbine control strategy at lower wind velocity based on neural network PID control. In Proceedings of the International Workshop on Intelligent Systems and Applications (ISA '09), Wuhan, China, 23–24 May 2009; pp. 1–5.
19. Perng, J.W.; Chen, G.Y.; Hsieh, S.C. Optimal pid controller design based on PSO-RBFNN for wind turbine systems. *Energies* **2014**, *7*, 191–209.
20. Phan, D.C.; Yamamoto, S. Maximum Energy Output of a DFIG Wind Turbine Using an Improved MPPT-Curve Method. *Energies* **2015**, *8*, 11718–11736.
21. Li, T.; Feng, A.J.; Zhao, L. Neural network compensation control for output power optimization of wind energy conversion system based on data-driven control. *J. Control Sci. Eng.* **2012**, *2012*, 736586.
22. Thongam, J.S.; Bouchard, P.; Ezzaidi, H.; Ouhrouche, M. Artificial neural network-based maximum power point tracking control for variable speed wind energy conversion systems. In Proceedings of the 18th IEEE International Conference on Control Applications, Part of 2009 IEEE Multi-conference on Systems and Control, Saint Petersburg, Russia, 8–10 July 2009; pp. 1667–1671.
23. Ganjefar, S.; Ghassemi, A.A.; Ahmadi, M.M. Improving efficiency of two-type maximum power point tracking methods of tip-speed ratio and optimum torque in wind turbine system using a quantum neural network. *Energy* **2014**, *67*, 444–453.
24. Aissaoui, A.G.; Tahour, A.; Abid, M.; Essounbouli, N.; Nollet, F. A fuzzy sliding mode-based power control design for wind turbine. In Proceedings of the 2012 2nd International Symposium on Environment-Friendly Energies and Applications (EFEA), Newcastle upon Tyne, UK, 25–27 June 2012; pp. 329–335.
25. Yao, X.; Liu, Y.; Guo, C. Adaptive fuzzy sliding-mode control in variable speed adjustable pitch wind turbine. In Proceedings of the IEEE International Conference on Automation and Logistics (ICAL '07), Jinan, China, 18–21 August 2007; pp. 313–318.
26. Abdeddaim, S.; Betka, A. Optimal tracking and robust power control of the DFIG wind turbine. *Int. J. Electr. Power Energy Syst.* **2013**, *49*, 234–242.

27. Kairous, D.; Wamkeue, R. DFIG-based fuzzy sliding-mode control of WECs with a flywheel energy storage. *Electr. Power Syst. Res.* **2012**, *93*, 16–23.
28. Boulâam, K.; Boukhelifa, A.A. Fuzzy sliding mode control for DFIG-based wind turbine power maximisation. In Proceedings of the 7th IET International Conference on Power Electronics, Machines and Drives (PEMD '14), Manchester, UK, 8–10 April 2014; pp. 1–6.
29. Tanvir, A.A.; Merabet, A.; Beguenane, R. Real-Time Control of Active and Reactive Power for Doubly Fed Induction Generator (DFIG)-Based Wind Energy Conversion System. *Energies* **2015**, *8*, 10389–10408.
30. Xu, L. Coordinated control of DFIG's rotor and grid side converters during network unbalance. *IEEE Trans. Power Electron.* **2008**, *23*, 1041–1049.
31. Singh, B.; Naidu, S.; Krishna, N. Direct power control of single VSC-based DFIG without rotor position sensor. *IEEE Trans. Ind. Appl.* **2014**, *50*, 4152–4163.
32. Zarei, M.E.; Asaei, B. Combined vector control and direct power control methods for DFIG under normal and unbalanced and distorted grid voltage conditions. In Proceedings of the 4th Power Electronics, Drive Systems and Technologies Conference (PEDSTC), Tehran, Iran, 13–14 February 2013; pp. 107–112.
33. Khedher, A.; Khemiri, N.; Mimouni, M.F. Wind energy conversion system using DFIG controlled by backstepping and sliding mode strategies. *Int. J. Renew. Energy Res.* **2012**, *2*, 421–430.
34. Liu, Y; Wu, Q.H.; Zhou, X.X.; Jiang, L. Perturbation observer based multiloop control for the DFIG-WT in multi-machine power system. *IEEE Trans. Power Syst.* **2014**, *29*, 2905–2915.
35. Balogun, A.; Ojo, O.; Okafor, F. Decoupled direct control of natural and power variables of doubly fed induction generator for extended wind speed range using feedback linearization. *IEEE J. Emerg. Sel. Top. Power Electron.* **2013**, *1*, 226–237.
36. Chen, G.; Zhang, L.; Cai, X. Optimized Control of the Doubly Fed Induction Generator System Based on input-output Linearizing Scheme. *Wind Eng.* **2014**, *38*, 101–108.
37. Nemmour, A.; Abdessemed, R. The input-output linearizing control scheme of the doubly-fed induction machine as a wind power generation. *Wind Eng.* **2008**, *32*, 285–297.
38. Balogun, A.; Ojo, O.; Okafor, F.; Karugaba, S. Determination of steady state anddynamic control laws of doubly-fed induction generators using natural and power variables. *IEEE Trans. Ind. Appl.* **2013**, *49*, 1343–1357.
39. Balogun, A.; Ojo, O.; Okafor, F. Decoupledcontrol of natural and power variables of doubly-fed induction generator using feedback linearization. In Proceedings of the 2012 IEEE Energy Conversion Congress and Exposition (ECCE), Raleigh, NC, USA, 15–20 September 2012; pp. 801–808.
40. Mauricio, J.; Leon, A.; Gomez-Exposito A.; Solsona, J. An adaptive nonlinear controller for DFIM-based wind energy conversion systems. *IEEE Trans. Energy Convers.* **2008**, *23*, 1025–1035.
41. Wu, F.; Zhang, X.; Ju, P.; Sterling, M. Decentralized nonlinear control of wind turbine with doubly fed induction generator. *IEEE Trans. Power Syst.* **2008**, *23*, 613–621.
42. Kamal, E.; Aitouche, A.; Ghorbani, R.; Bayart, M. Robust nonlinear control of wind energy conversion systems. *Int. J. Electr. Power Energy Syst.* **2013**, *44*, 202–209.
43. Kamal, E.; Oueidat, M.; Aitouche, A.; Ghorbani, R. Robust Scheduler Fuzzy Controller of DFIG Wind Energy Systems. *IEEE Trans. Sustain. Energy* **2013**, *4*, 706–715.
44. Isidori A. The zero dynamics of a nonlinear system: From the origin to the latest progresses of a long successful story. *Eur. J. Control* **2013**, *19*, 369–378.